meteorology

MDPI

Article

Intensity Measurements of a Landfalling Tropical Cyclone Using Conventional Coastal Weather Radar

Boris S. Yurchak

Retired Scientist, Previously with NASA Goddard Space Flight Center, Greenbelt, MD 20771, USA; bsyu33@gmail.com

Abstract: Tropical cyclone (TC) intensity observations considerably improve forecast models. They are particularly used to continuously measure TC intensity for landfalling cyclones to improve their forecast. For example, TC Irving, which operated in the Gulf of Tonkin, South China Sea, on 23–24 July 1989, was observed by a conventional weather radar installed at the Phu Lien Observatory in North Vietnam. The maximum wind speed was calculated by the hyperbolic-logarithmic approximation (HLS-approximation) of spiral cloud-rain bands (SCRBs) of recorded TC radar images. The data spanned about 15 h. Ground-based estimates of the cyclone intensity were obtained from pressure measurements at two coastal weather stations. A comparison of these estimates with the HLS wind resulting from the HLS approximation of SCRBs showed satisfactory synchronization. In particular, radar and meteorological data indicated cyclone intensification near landfall and rapid cyclone intensification after landfall. Both intensifications were accompanied by polygonal eye shapes. This study demonstrates the feasibility of using the HLS-approximation technique for retrieving TC intensity variation from conventional weather radar data.

Keywords: tropical cyclone; weather radar; HLS wind; intensity variation; rapid intensification

Citation: Yurchak, B.S. Intensity Measurements of a Landfalling Tropical Cyclone Using Conventional Coastal Weather Radar. *Meteorology* **2022**, *1*, 113–126. https://doi.org/10.3390/meteorology1020007

Academic Editor: Paul D. Williams

Received: 2 February 2022
Accepted: 28 February 2022
Published: 23 March 2022

1. Introduction

Tropical cyclones (TC) are one of the main natural factors causing material damage and loss of life on the islands and coastal regions of states located in the range of approximately 5–25 degrees latitude on both sides of the equator (e.g., [1]). The constant or frequent monitoring (satellite, radar, aircraft) of this dangerous natural phenomenon becomes more relevant to identify both the location of the TC center ashore and changes in TC intensity, especially a possible sudden intensification, as a TC approaches the coast [2]. Although the contemporary TC forecast models have notable achievements, they rarely predict rapid intensity changes [3]. Some research proposes to incorporate remote sensing observations into these models to improve their ability to predict TC intensity [4]. The radar method is a way to monitor a TC approaching a coast in real time. It meets the requirements of practical continuity. Typically, the eye of a cyclone, the size of its cloud field, and wind speed in the case of Doppler radar are monitored (e.g., [5–7]). Although coherent (Doppler) weather radars are gaining popularity (e.g., [8]), determining TC intensity change by its mesostructural characteristics, for example, eye (e.g., [9,10]), or, as suggested in this paper, by spiral cloud-rain bands, increases the reliability of intensity prediction. In addition, reconstructing the horizontal wind field from Doppler measurements requires two radars, additional physical assumptions, or the use of a special ground-based velocity track display (GBVTD) technique [6].

The accumulated archives of radar data in the form of sequential images of cloudy rain fields of TCs recorded on film or on other media represent a valuable source of historical information about TCs, that can be useful in climate research. These data can be used in conjunction with the Doppler data to improve intensity estimates. However, until recently it was not possible to extract from conventional (non-Doppler) radar data quantitative information about the change in the intensity of a cyclone as it approached the coast.

This work aims to illustrate the possibility of tracking changes in the maximum wind speed of a TC based on the archived data of a conventional weather radar using the recently developed hyperbolic-logarithmic approximation (HLS-approximation) of spiral cloud-rain bands (SCRB) of TC (e.g., [11,12]). The method is based on the Rankine vortex model and the theoretically found dependence of the characteristics of the SCRB on the maximum wind speed. This dependence, especially, explains the experimentally observed effect of rounding the cyclone core (decreasing crossing angle) with an increase in its intensity (e.g., [13–15]). Since the rationale of the HLS approximation and examples of its verification with data from direct airborne soundings have been already published (e.g., [11,12,16,17]), only the essence of this method is placed in Appendix A. Previous results have indicated the proximity of the maximum wind speed according to the HLS approximation of the archived radar data of the coastal radar of the Gulf of Mexico [17], as well as Puerto Rico's island radar installed in the city of San Juan [12], to the results of airborne soundings. This made it possible to start processing radar data obtained by the MRL-5 weather radar installed at the Vietnamese Phu Lien observatory (Supplementary Material S1). The observatory is built at a height of 116 m on Dau Son mountain, located in Kien An, an urban district of Haiphong city. The distance to the sea is about 15 km. In the period from 1989 to 1991, 13 TCs entered the surveillance zone of the radar, among which TC Irving was the strongest, with a well-organized spiral structure and a visible eye during a long period of its tracking. In this regard, data from the radar tracking of TC Irving (8910), which passed to the north of Vietnam from the Gulf of Tonkin on 23–24 July 1989, were used. At this time, the TC was a severe tropical storm (STS) on the tropical cyclone scale of the Regional Specialized Meteorological Center (RSMC) of the Japan Meteorological Agency (JMA).

The primary material for the current processing was a set of TC images from the plan position indicator (PPI) of the radar in the period from 19:00 (local time, (LT) = UTC + 7) on 23 July to 10:00 LT on 24 July 1989 (Supplementary Material S2). The TC was monitored by the radar over the sea, during landfall and over land. An additional method of processing is comparing the results of determining the maximum wind speed using the HLS approximation with the estimates of the surface maximum wind speed in the TC from the measured pressure at two coastal weather stations. This technique helped obtain independent estimates of the dynamics of the TC intensity over time for comparison with the results of the HLS approximation, which was previously performed only from aircraft data (e.g., [16,17]).

2. TC Evolution over the Observation Period

2.1. TC Track in the Radar Surveillance Zone

The track of the TC center in the radar surveillance zone is shown in Figure 1 by 14 points corresponding to the observation period from 19:30 LT on 23 July to 9:48 LT on 24 July 1989.

In Figure 1, dots 1–4 correspond to the position of the TC center at 19:30, 21:20, 22:15, and 23:15 on 23 July and dots 5–14 correspond to the positions of the TC center at 00:14, 01:30, 02:15, 03:45, 04:45, 06:15, 07:14, 08:18, 09:15, and 09:48, respectively, on 24 July. Letters A, B, C, and D denote the dots of the Best Track corresponding to the position of the TC center at 1200 UTC, 23 July (19:00 LT, July 23), 1800 UTC, 23 July (01:00 LT 24 July), 0000 UTC, 24 July (07:00 LT, 24 July), and 0600 UTC, 24 July (13:00 LT, 24 July), respectively (Supplementary Material S3). The triangle marks the position of the radar near the city of Haiphong. The superimposed radar image of the TC corresponds to the position of the TC center at dot 7 (02:15 LT); the background Vietnam satellite image source-interactive map of Vietnam is available at: https://www.google.com/maps/place/Do+Son+Beach/@20.2269053,106.2900628,11z/data=!4m5!3m4!1s0x314a6c608b8feabd:0x5bf0cbf27e7679c2!8m2!3d20.6872771!4d106.7954793; accessed on 20 December 2021.

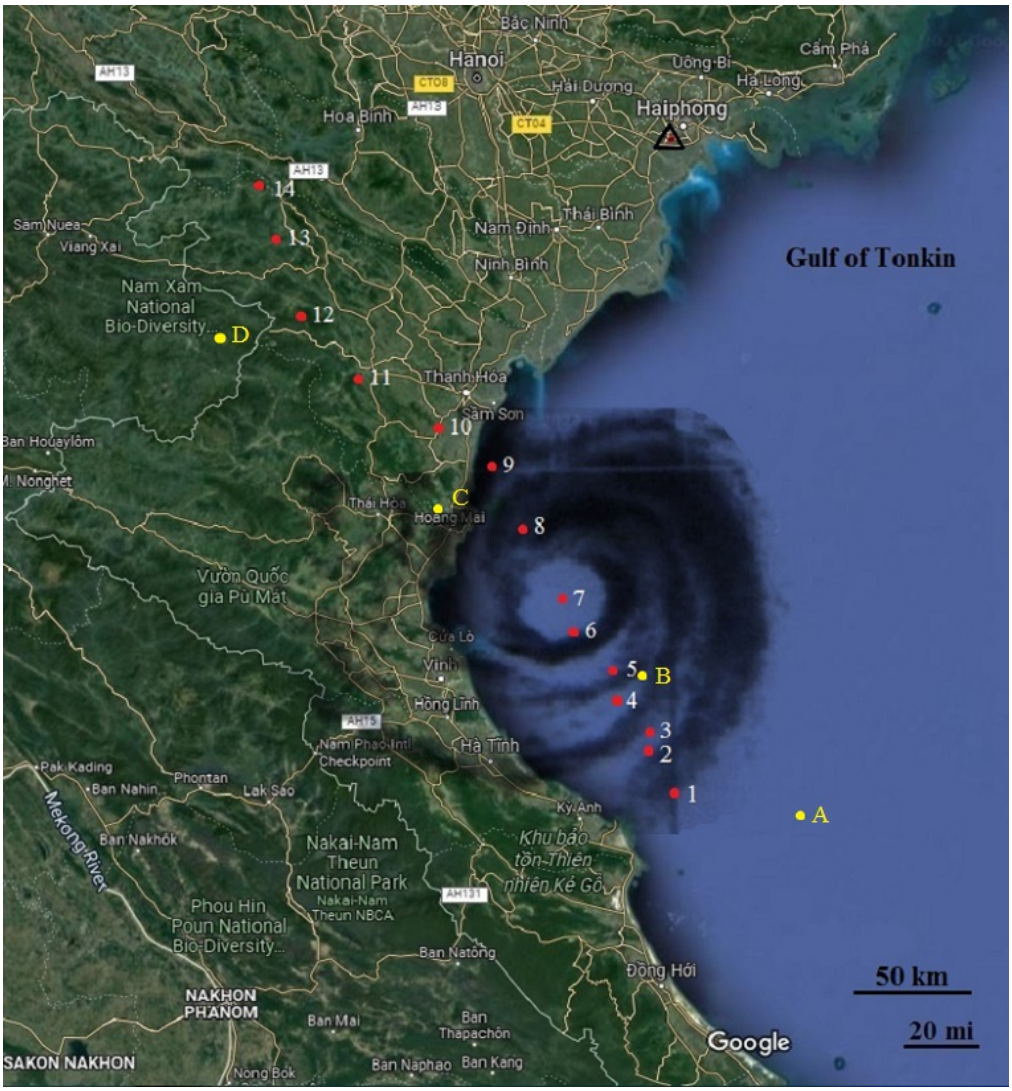

Figure 1. Track of TC Irving on 23–24 July 1989 in the Gulf of Tonkin according to the weather radar installed at the Phu Lien Observatory (indicated by numbered red dots). Remaining explanations are in the text.

The surveillance began at a distance to the center of the TC of 285 km in the Gulf of Tonkin and ended at a range of about 180 km (when the cyclone was approximately 150 km from the coast). At the entrance to the Gulf of Tonkin from 19:30 LT on 23 July to 0:14 LT on 24 July (dots 1–5), the distance from the TC center to the coast gradually increased from 26 to 60 km. From 0:14 to 2:30 LT on 24 July (dots 5–7), the distance was about 50–60 km. Figure 1 also shows the radar image of the TC center at 2:15 LT (dot 7) for an illustration. Until this moment, on 24 July, the cyclone had moved approximately along the coast; then it began to approach the coastline. The landfall of the TC center took place near the city of Thanh Hoa at approximately 5:30 LT on 24 July, after which the cyclone began to move further to the northwest (dots 10 and 11) and then almost to the north (dots 12–14). The cyclone dissipated at about 10:00 LT at a distance of about 150 km from the coast (dot 14).

2.2. Estimation of TC Intensity Variation Based on the Results of HLS Approximation of Radar Images of Spiral Cloud-Rain Bands

To estimate the variation in TC intensity, the HLS approximation technique (e.g., [17]) was applied to 42 images from PPI (Supplementary Material S2).

The results of calculation of the maximum wind speed of a cyclone when it approaches the coast (and makes landfall) are shown in Figure 2. The graph shows the main period

of cyclone intensification from approximately 1:00 to 5:00 LT on 24 July, during which the average wind speed varied within the range of 40–60 m s^{-1}. After the TC center moved ashore at 5:30–6:00 LT, the wind speed increased to about 58 m s^{-1}, and then dropped at 7:40 LT to approximately 20 m s^{-1}, after which, there was a burst of intensity (up to 49 m s^{-1}) from 8:48 to 9:15 LT, followed by a decrease (to 18 m s^{-1}) by 9:48 LT. Therefore, a characteristic feature of the TC intensity profile was the presence of two intensifications, the first of which occurred when the TC center was located above the sea and the second when it was over land.

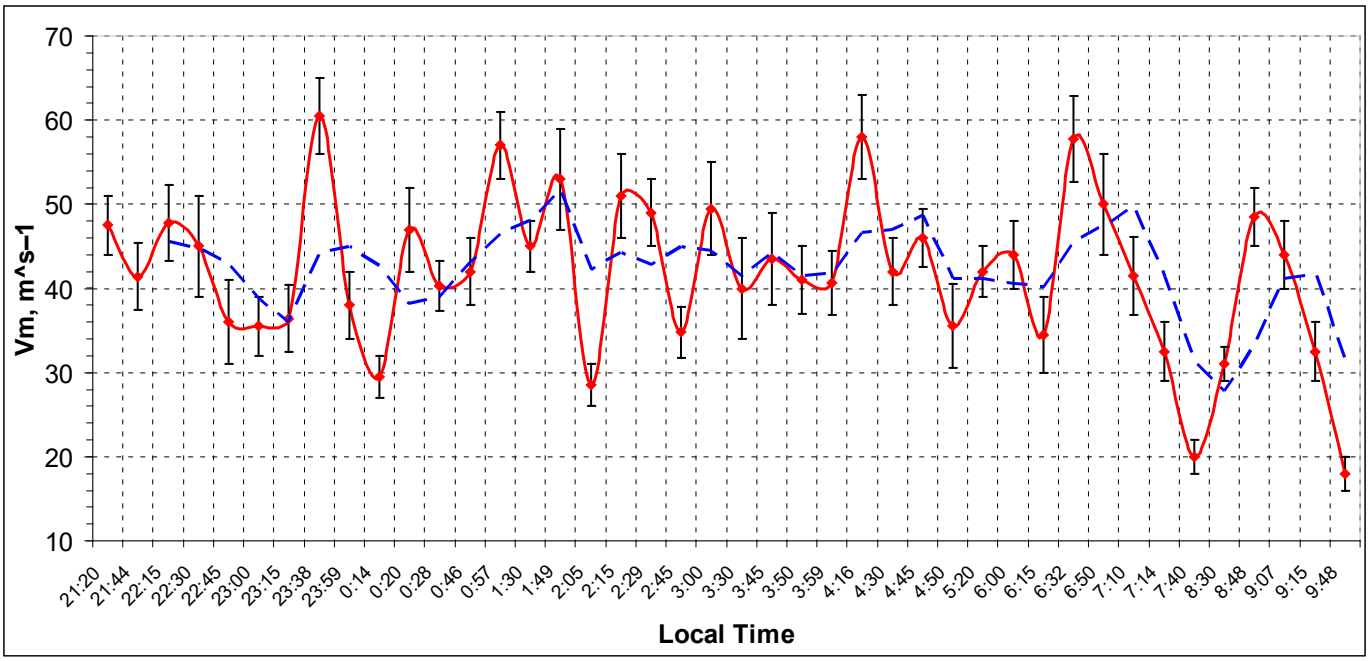

Figure 2. Change in the maximum wind speed in the TC, obtained by HLS approximation of radar images of spiral cloud-rain bands; the dashed blue curve is the result of moving average of point data over three points; local time from 21:20 to 23:15 refers to 23 July 1989, other time points refer to 24 July 1989.

The estimation of TC intensity by means of HLS approximation is a relatively new technique. Therefore, the results obtained should be compared with independent measurements. Earlier, in the above-mentioned works of the author [12,16,17], such a comparison, as a rule, was carried out with the data of the aircraft sounding of the TC. In the case under current consideration, such a possibility was absent and, therefore, an attempt was made to obtain data on the change in TC intensity from pressure data of coastal weather stations. The corresponding approach is discussed below.

3. Estimation of the Central Pressure and Maximum Surface Wind Speed in the TC according to the Data of Two Coastal Weather Stations

3.1. Basic Relations and Estimation Algorithm

According to [18], the pressure at a point located at a distance R from the center of the TC on the surface is:

$$P(R) = P_c + (P_n - P_c)\exp\left(-\frac{A}{R^\beta}\right) \quad (1)$$

where P_c is the pressure at the center of the TC on the surface, P_n is the external pressure (outside the influence of the cyclone), A and β are scale parameters that determine the maximum wind radius (MWR):

$$R_m = A^{1/\beta} \quad (2)$$

Considering Equation (2), Equation (1) can be represented as

$$P(R) = P_c + (P_n - P_c) \exp\left[-\left(\frac{R_m}{R}\right)^{\beta}\right] \quad (3)$$

In the presence of data from two weather stations, the following combined equation can be drawn up to calculate the pressure at the center of the TC under the assumption of an axisymmetric pressure distribution:

$$P_n Z(\beta)_1 = P_C = P_n Z(\beta)_2 \quad (4)$$

where

$$Z(\beta)_1 = \frac{\frac{P_1(R_1)}{P_n} - \exp\left[-\left(\frac{R_m}{R_1}\right)^{\beta}\right]}{1 - \exp\left[-\left(\frac{R_m}{R_1}\right)^{\beta}\right]} \quad (5)$$

and

$$Z(\beta)_2 = \frac{\frac{P_2(R_2)}{P_n} - \exp\left[-\left(\frac{R_m}{R_2}\right)^{\beta}\right]}{1 - \exp\left[-\left(\frac{R_m}{R_2}\right)^{\beta}\right]} \quad (6)$$

In Equations (4)–(6), parameters with indices 1 and 2 are of the first and second weather stations, respectively. The graphical solution of the reduced combined Equation (4)

$$Z(\beta)_1 = Z(\beta)_2 \quad (7)$$

as the intersection points of the functions $Z(\beta)_1$ and $Z(\beta)_2$ (calculated considering the radius of maximum winds R_m and distances R_1 and R_2 from the cyclone center to the weather stations #1 and #2 measured by the radar method) makes it possible to determine the unknown value of the scale parameter β and then calculate the value of the pressure in the center of the TC using the right or the left side of the combined Equation (4).

In the present study, the radius of the zone of maximum winds was measured from the radar image of the cyclone on the PPI as the distance from the center of the eye to the middle of the most intense part of the eyewall corresponding to the maximum convection.

Although these data refer to the radius of maximum wind of the TC horizontal cross-section at the height of a radar beam, an analysis of the vertical cross sections of several hurricanes given in [19] shows that the region of maximum reflectivity of the convective ring is oriented almost vertically from an altitude of about 6 km to the surface. Therefore, in this work, no correction was made for a possible decrease in the radius of the maximum wind near the surface.

3.2. The Results of Calculating the Surface Pressure in the Center of the TC

In our case, weather stations 1 and 2 were located in the cities of Thanh Hoa and Vinh. The assessments according to the proposed algorithm were facilitated by the fact that the center of the TC arrived at the coast between these cities (23 km south of Thanh Hoa and 92 km north of Vinh); see Figure 1. The initial data and the results of calculating the pressure in the center of the TC according to the above algorithm are shown in Table 1. As follows from this table, it was not possible to solve Equation (7) at the beginning of the tracking when the TC center was located at a distance of about 112 km from Vinh and 193 km from Thanh Hoa, as well as for data at 3:45 and 4:45 LT (dots 8 and 9 in Figure 1), apparently because the interaction of the zone of maximum winds and the coast violated the symmetry condition for the distribution of the pressure field at this time.

Table 1. Surface pressure calculation results at the center of TC Irving.

Date, 1989 Year	Dot #	Local Time	Sampled Pressure (Interpolated) at Weather Station, hPa		Distance (km) to TC Center from		Radar Measured MWR, R_m, km	Calculated Parameters	
			Vinh	Thanh Hoa	Vinh	Thanh Hoa		β	P_c, hPa
July 23	1	19:30	996.50	996.30	112	193	27	No solution	
	2	21.20	996.90	1000.00	94	173	48	0.49	981.6
	3	22:15	997.00	1000.00	94.5	168.6	28.3	0.465	976.2
	4	23:15	996.75	1000.15	77.5	149.6	28.2	0.475	977.8
July 24	5	0:14	995.75	999.05	75.4	137.0	27.2	0.63	970.8
	6	1:30	994.50	997.10	***61.7***	114.6	31.3	0.355	970.8
	7	2:15	993.65	997.10	63.8	98.2	21.5	0.58	***966.1***
	8	3:45	***993.13*** [1]	995.90	74.1	64.8	27.7	No solution	
	9	4:45	994.30	994.40	94.5	34.8	29.8	No solution	
	10	6:15	995.05	989.60	108.4	***20.5***	24.7	0.24	977.4
	11	7:14	995.65	985.70	134.6	47.6	23.6	0.565	957.4
	12	8:18	996.30	***984.30***	168.8	78.9	29.1	0.84	931.2
	13	9:15	997.00	988.50	204.1	106.2	26	0.75	***929.7***
	14	9:48	997.10	991.40	228.5	127.3	20	0.6	936.2

[1] Minimum pressures and distances are shown in italics and bold.

3.3. Estimation of the Maximum Surface Wind Speed in the TC Based on the Data of Combined Meteorological and Radar Measurements

After determining the pressure in the center of the cyclone and the radius of the zone of the maximum wind speed, performed in the previous section, it is possible to estimate the maximum near-surface wind speed, the most important characteristic of the TC from a practical point of view when the TC approaches the coast (and makes landfall). For this, the results of [18] can be used again. In particular, the distance distribution of the tangential surface velocity in a cyclone is determined by:

$$V(R) = 10\sqrt{\left(\frac{A}{R^{\beta}}\right)\beta\frac{P_n - P_c}{\rho}\exp\left(-\frac{A}{R^{\beta}}\right)} \quad (8)$$

where ρ is the air density equal to 1.15 kg m^{-3}; the rest of the parameters are defined earlier in Section 3.1.

Equation (8) differs from the same in the original paper [18] by a factor of 10. This follows from the analysis of dimensions in the ratio of the pressure drop $(P_n - P_c)$ to the air density (ρ) if the pressure drop is in millibars (mb) or hectopascals (hPa) and the air density is in kilograms per cubic meter (kg m^{-3}).

The maximum wind speed takes place at $R = R_m$. Considering Equations (2) and (8), one obtains for different times t_i:

$$V(t_i)_m = 10\sqrt{\beta(t_i)\frac{\Delta P(t_i)}{\rho \cdot e}} \quad (9)$$

where e is the base of the natural logarithm.

The maximum surface wind speed calculated using this formula and the data in Table 1, together with the measured surface wind speed at the Thanh Hoa weather station to the center of the TC, is shown in Figure 3.

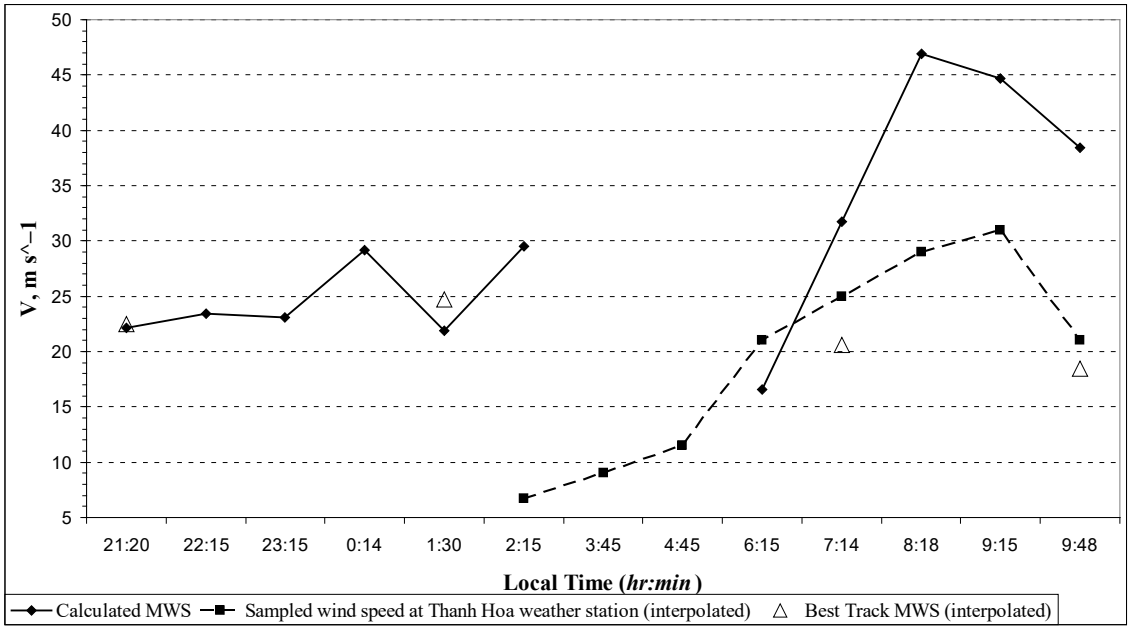

Figure 3. Maximum surface wind speed in the TC calculated from data of combined meteorological and radar measurements and data of Thanh Hoa weather station.

3.4. Verification the Calculated Maximum Surface Wind Speed from Measurements at a Weather Station and Best Track Data

The calculated maximum surface wind from the combined radar–meteorological data was verified by comparing these results with the interpolated measured values of the surface wind at the Thanh Hoa weather station (Figure 3). The comparison was made with weather data corresponding to the position of the TC center near this meteorological station (dots 10 and 11 on the TC track, respectively; Figure 1) and with the Best Track data interpolated in time to the measuring time points also presented in Figure 3. The comparison shows that at approximately 6:45 LT (middle position between dots 10 and 11), the calculated maximum wind speed coincides with the measured one, when the maximum TC wind zone approximately covered the weather station. After this zone completely reaches the coast, the maximum wind speed in the TC begins to prevail over the wind speed measured at the weather station in proportion to the distance of the maximum wind zone from the weather station (dots 11–14). Both surface wind plots in Figure 3 show short-term secondary TC intensification over land between approximately 06:15 and 09:15 LT.

The Best Track data interpolated to the measuring points show almost complete agreement with the calculated values of the maximum wind before the TC landfall (dots 2 (21:20 LT) and 6 (1:30 LT)) and a satisfactory agreement with the measured values of the surface wind at Thanh Hoa station after the TC center landed (dots 11 at 7:14 LT and 14 at 9:48 LT). Thus, the method used for calculating the maximum surface wind leads to a satisfactory agreement with the measured meteorological parameters. However, a comparison of the Best Track data with the calculated values of the maximum wind at these time points shows a significant discrepancy. Apparently, the calculation of the wind for Best Track considered only the Thanh Hoa weather station data. The 6 h interval inherent to the Best Track data also did not reveal the secondary intensification of the TC.

4. Discussion

The purpose of the following discussion is to evaluate the support for the change in TC intensity identified by the HLS approximation of SCRBs with other sources of information available in this study such as Best Track data, estimated maximum surface wind speed from pressure data from two coastal weather stations, and data on changing shape of the

TC eye. For brevity, the HLS estimates of the maximum wind are hereinafter referred to as "HLS-wind". Due to the noted difference in altitudes of the HLS-wind and the surface wind, the presence of a change in the TC intensity over the observation period is taken as the primary criterion for data similarity. As follows from Figure 2, the HLS-wind demonstrates two intensification events. The first intensification took place when the TC center was located above the sea approximately from 1:00 to 5:00 LT on 24 July. During this period, the average wind speed varied within 40–60 m s^{-1}. After the TC center came ashore at 05:30 LT, the wind speed demonstrated a fluctuation from 40 to 58 m s^{-1}, then decreased noticeably to approximately 20 m s^{-1} at 07:40 LT, after which there was a surge in the secondary intensity (up to 50 m s^{-1}) from 8:30 to 9:15 LT, followed by a decrease (to 18 m s^{-1}) by 9:48 LT. The course of the calculated maximum surface wind speed shown in Figure 3 also shows an increase in speed from approximately 23 to 30 m s^{-1} in the period from 23:15 LT on 23 July to 2:15 LT on 24 July, which corresponds to the period of the first HLS-wind intensification.

The second, even more intense TC intensification over land is also clearly visible in the graph (Figure 2). It started at 06:15 LT and lasted until 08:18–09:15 LT. Thus, the course of the calculated maximum wind speed does not contradict the behavior of the HLS-wind. It can be assumed that such fluctuations in the TC intensity are due to the specific temperature regime of the coastal water area.

The ratio between the surface calculated maximum wind speed V_{cal} (Figure 3) and the HLS-wind V_{HLS} (Figure 2) varied depending on the position of the TC center. At the beginning of tracking, from 21:20 LT (dot 1) on 23 July to 2:15 LT (dot 7) on 24 July, the V_{cal}/V_{HLS} ratio was approximately 25/40. From 2:15 to 6:15 LT (dot 10), this ratio could not be established due to the impossibility of calculating V_{cal}.

In the final period from 6:15 to 9:48 LT, the maximum values of this ratio fluctuated approximately from 16/58 to 43/48, i.e., during the secondary intensification, both velocities turned out to be practically the same, regardless of the altitude difference for which these estimates were made. The ratio for the initial period can be explained by the significant altitude of the radar signatures, used to make HLS estimates of the maximum wind. For this period, the altitude of the radar beam was approximately 6.5 to 4 km (Appendix B), where the wind speed was probably greater than the surface speed. During the final period, the altitude of the radar beam was approximately 3 to 3.5 km (Idem). Therefore, the proximity of the considered wind speeds can, apparently, be attributed to the case when the TC was already a relatively barotropic vortex. In this case, the vertical profile of the tangential wind changed little with altitude. This, in particular, was observed in hurricane Gloria (1985) below the level of 450 mb (~6 km) [20].

As noted in Section 3.4, due to the 6 h interval, the secondary TC intensification was not presented in the Best Track data. However, the data for 1800 UTC on 23 July (01:00 LT 24 July) on pressure (975 hPa) given in Table 2 indicate the presence of the primary TC intensification coinciding with the beginning of the corresponding HLS-wind intensification.

Interpolated to the nearest measurement point at 01:30 LT, the Best Track data showed the minimum pressure 975.8 hPa compared to a calculated pressure of 970.8 hPa at that time. The minimum calculated pressure at 2:15 LT, under the first intensification was 966.1 hPa and at 09:15 LT, during the secondary intensification, was 929.7 hPa; Table 1. The secondary intensification is clearly identified in Figure 2 by the HLS-wind diagram but omitted in the Best Track data. The noted circumstances emphasize the importance of continuous monitoring of changes in the intensity of landfalling TCs.

Additional qualitative information about the intensity of a cyclone can also be obtained by observing of the configuration of the TC eye. As shown in recent studies (e.g., [5,7,9,10]), the intensification of TCs is accompanied by irregular polygonal eye configurations. The same was observed in the TC being discussed. Six polygonal eye samples are presented in Figure 4. From Figures 1 and 4, it follows that the polygonal eye shape appeared both during the first intensification (the image at 02:15 LT in Figure 1 and images in the upper

row from 1:48 to 4:45 LT in Figure 4) and the second one (images in the lower row from 6:15 to 8:13 LT in Figure 4). In the latter case, a rather rare triangular eye shape was observed at 8:13 LT, before the TC dissipation. Thus, both intensification events identified by the HLS approximation of SCRBs are also confirmed by the reported qualitative characteristics of the TC eye shape. The TC eye configurations were determined by the radar at the same altitude as the SCRB location, which was used to determine the HLS wind.

Table 2. Best Track pressure and wind data for TC Irving (8910) over the observation period (according to [21]).

Best Track Data (Extracted from Original)				Nearest Dot and Time Point		Interpolated Values at Time Points	
Time/Date 1989 Year		Minimum Central Pressure, hPa	Maximum Surface Wind, m s^{-1}	Dot #	Local Time and Date	Minimum Central Pressure, hPa	Maximum Surface Wind, m s^{-1}
UTC	Local (UTC + 7)						
1200 7/23	19:00 7/23	985	21	1	19:30 7/23	984.2	21.3
				2	21:20 7/23	981.2	22.5
1800 7/23	01:00 7/24	975	25	6	01:30 7/24	975.8	24.7
0000 7/24	07:00 7/24	985	21	11	07:14 7/24	985.4	20.6
0600 7/24	13:00 7/24	995	16	14	09:48 7/24	990.0	18.5

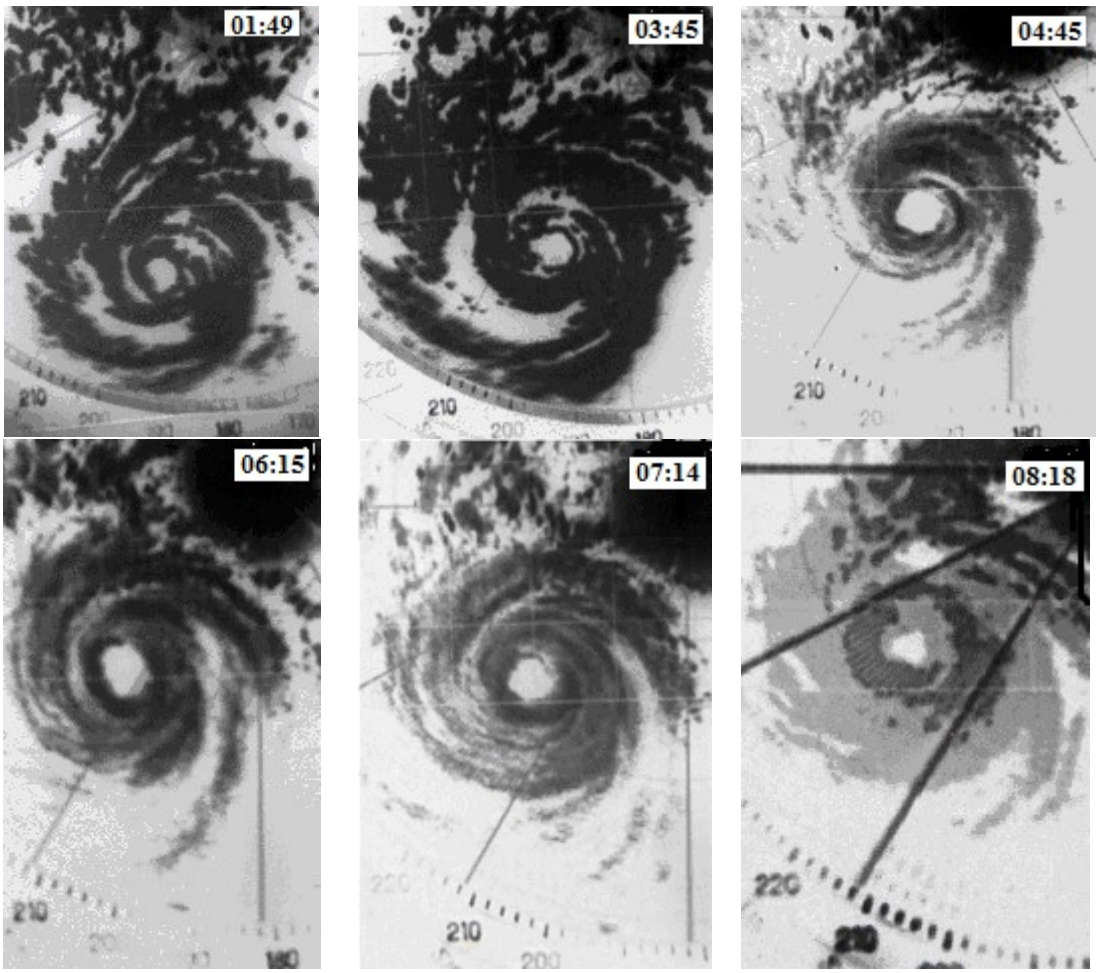

Figure 4. Examples of TC Irving polygonal eye shape observed on 24 July 1989; local time is printed in upper right corner of images.

5. Summary

Historical materials on radar surveillance of TC Irving (8910), which operated in the Gulf of Tonkin, South China Sea, on 23–24 July 1989, were used to assess the change in the intensity of a TC as it approached the coast, made landfall, and passed over land. The maximum wind speed was determined by approximating the recorded radar images of spiral cloud-rain bands (SCRBs) with a hyperbolic-logarithmic spiral (HLS). For comparison with ground-based measurements and the Best Track assessments, the minimum pressure and maximum surface wind speed in the cyclone were determined on the basis of pressure measurements by two coastal weather stations and data from radar measurements of the MWR and the distance from the center of the cyclone eye to the stations. A comparison of such ground-based estimates of the cyclone intensity with the results of the HLS-approximation of the SCRBs showed a satisfactory agreement of the temporal characteristics of changes in the cyclone intensity. Archived data of the radar tracking of the TC helped reconstruct the change in its intensity with a satisfactory time resolution (0.25–1 h), which made it possible to clarify the history of the intensity change in comparison with the standard 6 h analysis. In particular, the secondary short-term intensification of the TC was detected after the landfall. In addition, updated values of the maximum wind speed and intensification start/end time were obtained for the observation period both at the altitude of the radar beam and altitudes close the sea and land surfaces. The range of applicability of the HLS technique in estimating TC intensity is limited only by the maximum range of the radar.

Thus, this study illustrates the possibility of intensity changes from archived data by the HLS-approximation of the recorded radar signatures of SCRBs in the surveillance zone of the conventional coastal weather radar. The result obtained confirms the conclusion statement in [12] that the HLS approach to retrieve the TC's intensity is particularly beneficial for ground-based coastal radar probing of a TC before its landfall and the absence of aircraft reconnaissance missions. It seems that further improvement of the above methodology, tested here on archival materials, in combination with TC intensity measurements by other remote methods, will also improve the reliability of short-term forecasting of the intensity of a TC as it approaches the coast and makes landfall.

Supplementary Materials: The following supporting information can be downloaded at: https://www.mdpi.com/article/10.3390/meteorology1020007/s1, Supplementary Material S1 (MRL-5, Phu Lien Observatory), Supplementary Material S2 (Radar data), Supplementary Material S3 (Best Track data).

Funding: This research received no external funding.

Institutional Review Board Statement: Not applicable.

Informed Consent Statement: Not applicable.

Acknowledgments: The author expresses his gratitude to the leadership of the Vietnamese Weather Service and the Phu Lien Observatory for creating favorable conditions for this research and providing data from coastal weather stations, as well as the Vietnamese and Russian employees of the Central Aerological Observatory of Vietnam and the Joint Russian–Vietnamese Laboratory of Tropical Meteorology for their assistance in radar measurements. It is the author's pleasure to acknowledge valuable and useful comments by the four anonymous reviewers of the manuscript.

Conflicts of Interest: The author declares no conflict of interest.

Appendix A. The Principle of HLS-Assessment of Physical Characteristics of a Tropical Cyclone

TC intensity based on the representation of the streamline in the form of the hyperbolic-logarithmic spiral (HLS) is determined according to the hyperbolic distribution of the tangential velocity in the outer part of the Rankine vortex.

$$V(r) = V_m \left(r_m \frac{1}{r} \right)^n, \; r_m \leq r < \infty \tag{A1}$$

where r is the polar radius in the center of the cyclone, r_m is the radius of the maximum wind relative to which the vortex region is divided into internal and external parts, V_m is the maximum wind speed, $V(r)$ is the wind speed at a distance r from the center of the cyclone, n is the hyperbolic index.

Within the outer part of the vortex $n = 1$ for an ideal (theoretical) Rankine vortex, and the wind speed varies according to the hyperbolic law. A streamline for the external section of the Rankine vortex is described by the HLS in polar coordinates originating in the center of a TC [11,12]:

$$\varphi = A\left(\frac{1}{y^{n+1}} - 1\right) - B\ln y \equiv A\left\{e^{-(n+1)\ln y} - 1\right\} - B\ln y \tag{A2}$$

where φ is the polar angle and $y = r/r_0$ is the polar radius normalized to r_0 that is the conditional range of the beginning of a streamline that coincides with the range of the accepted reference point of the polar angle of the spiral (a point within a spiral signature).

In Equation (A2), coefficients A and B are determined by the following relationships:

$$A = \frac{r_m^n}{k(n+1)\,r_0^{n+1}} V_m \tag{A3}$$

and

$$B = \frac{f}{k} \tag{A4}$$

where k is the friction factor and f is the Coriolis parameter.

Thus, parameter A, which determines the difference between the HLS and the logarithmic spiral, is proportional to the maximum wind speed. The HLS reflects an increase in cyclone intensity, a decrease in the steepness of the spiral twist as it approaches the center of a TC. At this point, the configuration of the spiral adjacent to the central cloudy field of the TC increasingly degenerates into a circular arc. Equation (A2) shows that the HLS is close to the logarithmic spiral but only at the periphery of the cyclone, where the normalized polar radius is slightly less than 1. As one approaches the center of the cyclone, the spiral begins to "round off" (with constant k and n). The earlier (at a greater distance from the center) this happens, the higher the maximum wind speed.

Thus, as follows from the definitions of the HLS coefficients (Equations (A3) and (A4)), the maximum wind speed can be determined for given n, f, r_m, and r_0 as a function of approximate estimates of the coefficients $\hat{A}$ and $\hat{B}$ as follows:

$$V_m = \frac{\hat{A}}{\hat{B}}(n+1)\left(\frac{r_0}{r_m}\right)^n V_C \tag{A5}$$

where $V_C = r_0 f$ is a term with the dimension of speed; therefore, it is conventionally designated as the Coriolis velocity.

Coefficients A and B are determined through the assimilation approximation of a radar spiral band signature by the HLS. This HLS approximation consists of determining the "expected" (mean) spiral of a set of HLSs "fitted" into a pattern of the signature. The procedure is described in [16].

Appendix B. The Influence of Radio Refraction on Radar Probing of TCs

In radar sounding of TCs, it is desirable to know the altitude at which the radar beam intersects the TC mesoscale spiral structure in order to associate the measured wind with a specific vertical position in relation to the Earth surface (sea). In tropical conditions, knowing only the antenna elevation angle, antenna altitude and the measured distance to the TC center is not enough due to refractive effects that change the track of the radar beam of a finite angular size. For simplicity, the current consideration is limited to finding the parameters of the radar ray, that is, the axis of the radar beam.

The altitude of the radar ray H, considering the refraction and sphericity of the Earth, depending on the distance along the Earth's surface (s), is [22] (p. 29):

$$H(s) = \frac{\left[\frac{s\cdot(1-\gamma\cdot a)}{\cos\alpha} + a\cdot\sin\alpha\right]^2 - (a\cdot\sin\alpha)^2}{2a\cdot(1-\gamma\cdot a)} \quad \text{(A6)}$$

where $\gamma = \left|\frac{dn}{dh}\right|$ is the absolute value of the vertical gradient of the refractive index n (assuming that n decreases linearly of with altitude), $a = 6.37{\cdot}10^6$ m is the Earth's radius, α is the elevation angle of the radar antenna in transmit mode.

Equation (A6) does not consider the antenna height (h_0). For the case under consideration (radar MRL-5 installed at Phu Lien observatory), the altitude of the antenna center $h_0 \approx 140$ m.

To satisfy the condition $H(0) = h_0$, the final formula is

$$H(s)* = H(s) + h_0 \quad \text{(A7)}$$

At normal (standard) refraction, $dn/dh = -4{\cdot}10^{-8}$ m^{-1}. Conditions under which $dn/dh = -15.7\cdot10^{-8}\text{m}^{-1}$ correspond to the threshold refraction, at which the curvature of the radar ray coincides with the curvature of the Earth. In this case, the altitude of the radar ray is determined only by the distance to the selected point, the elevation angle, and the altitude of the antenna.

However, in tropical conditions, when the temperature difference between water and air is insignificant, the most typical is super-refraction, at which $-15.7\cdot10^{-8}\text{m}^{-1} \le dn/dh \le -4\cdot10^{-8}\text{m}^{-1}$, that is, the altitude of the radar ray also continues to increase non-linearly with increasing distance but not as fast as with standard refraction.

According to [23], July in Vietnam is characterized by refractivity $N = (n-1){\cdot}10^6 = 321$ with its gradient estimated from meteorological observations equal to $dN/dh = -4.58{\cdot}10^{-2}$ m^{-1}. Respectively, $dn/dh = -4.58\cdot10^{-8}$ m^{-1}. Therefore, there is super-refraction. The altitude of the radar ray therefore tends to increase non-linearly with increasing distance to the target (TC).

The radar ray path calculated by Equation (A7) in the range of 1–300 km at an elevation angle of 0.5 degrees is shown in Figure A1 for assumed survey conditions ($dn/dh = -4.58\cdot10^{-8}\text{m}^{-1}$), as well as for standard ($dn/dh = -4.0{\cdot}10^{-8}$ m^{-1}) and threshold ($dn/dh = -15.7\cdot10^{-8}\text{m}^{-1}$) comparative conditions.

The data from [23] should be considered only as a first approximation due to the lack of more detailed information about the real vertical profiles of temperature and humidity corresponding to the time and region of observations. There is evidence that the refractivity showed a sharp rise with the approach of the low pressure area due to the transport of moisture to a high altitude in severe TC, e.g., [24]. This issue needs further clarification.

The dependence of the distance from the location of the radar to the center of the TC on the observation time is shown in Figure A2.

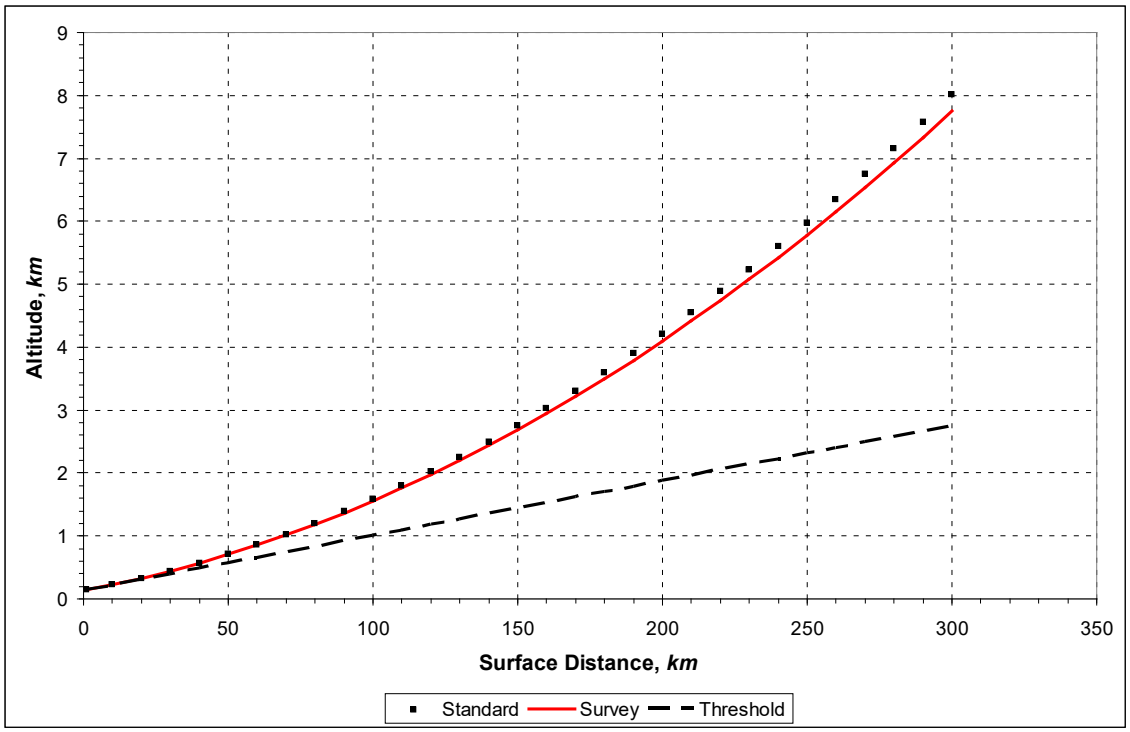

Figure A1. Radar ray path at antenna elevation angle of 0.5° for standard, threshold, and assumed survey conditions.

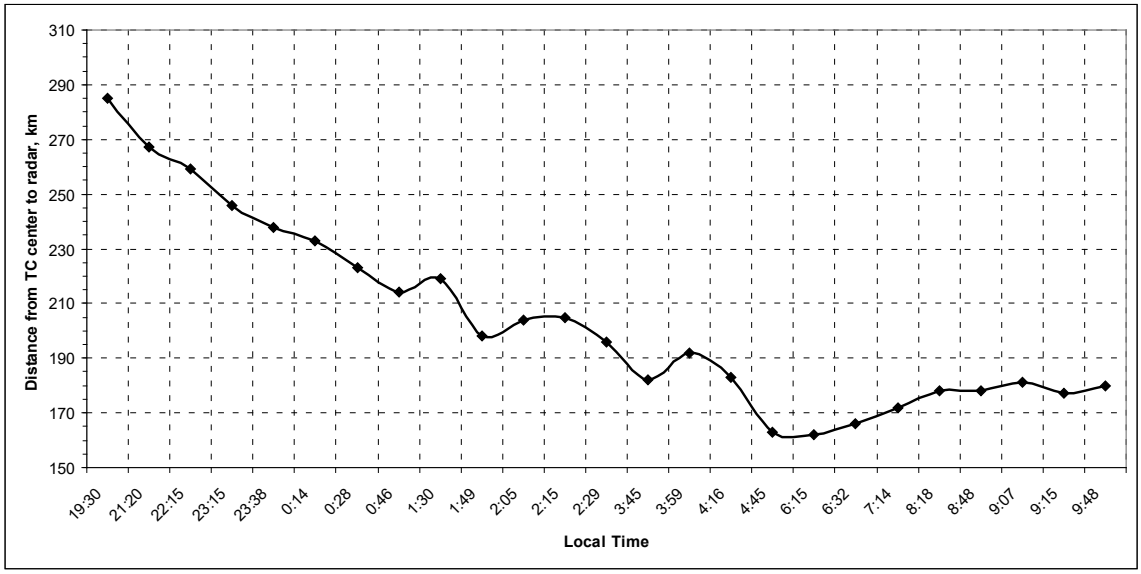

Figure A2. Changing the distance between the radar and the center of the TC. Note: The distance measured by the radar is slightly different from the surface distance used in Figure A1. For example, a roughly estimated discrepancy for the surface distance of 300 km is approximately 0.2 km or less. For closer places, this discrepancy is even smaller.

References

1. Rappaport, E.N. Fatalities in the United States from Atlantic Tropical Cyclones: New Data and Interpretation. *Bull. Am. Meteorol. Soc.* **2014**, *95*, 341–346. [CrossRef]
2. Emmanuel, K. 100 years of progress in tropical cyclone research. *Meteorol. Monogr.* **2018**, *59*, 15.1–15.68. [CrossRef]
3. Cangialosi, J.P.; Blake, E.; DeMaria, M.; Penny, A.; Latto, A.; Rappaport, E.; Tallapragada, V. Recent Progress in Tropical Cyclone Intensity Forecasting at the National Hurricane Center. *Weather Forecast.* **2020**, *35*, 1913–1922. [CrossRef]

4. Lu, X.; Wang, X. Improving Hurricane Analyses and Predictions with TCI, IFEX Field Campaign Observations, and CIMSS AMVs Using the Advanced Hybrid Data Assimilation System for HWRF. Part II: Observation Impacts on the Analysis and Prediction of Patricia (2015). *Mon. Weather Rev.* **2020**, *148*, 1407–1430. [CrossRef]
5. Zhu, X.; Li, Q.; Yu, J.; Wu, D.; Yao, K. Geometric Characteristics of Tropical Cyclone Eyes before Landfall in South China based on Ground-Based Radar Observations. *Adv. Atmos. Sci.* **2018**, *35*, 592–603. [CrossRef]
6. Lee, W.-C.; Jou, B.J.D.; Chang, P.-L.; Deng, S.-M. Tropical Cyclone Kinematic Structure Retrieved from Single-Doppler Radar Observations. Part I: Interpretation of Doppler Velocity Patterns and the GBVTD Technique. *Mon. Weather Rev.* **1999**, *127*, 2419–2439. [CrossRef]
7. Lee, W.-C.; Bell, M.M. Rapid intensification, eyewall contraction, and breakdown of Hurricane Charley (2004) near landfall. *Geophys. Res. Lett.* **2007**, *34*. [CrossRef]
8. Stith, J.L.; Baumgardner, D.; Haggerty, J.; Hardesty, R.M.; Lee, W.-C.; Lenschow, D.; Pilewskie, P.; Smith, P.L.; Steiner, M.; Vömel, H. 100 Years of Progress in Atmospheric Observing Systems. *Meteorol. Monogr.* **2018**, *59*, 2.1–2.55. [CrossRef]
9. Barnes, C.A.; Barnes, G.M. Eye and Eyewall Traits as Determined with the NOAA WP-3D Lower-Fuselage Radar. *Mon. Wea. Rev.* **2014**, *142*, 3393–3417. [CrossRef]
10. Cha, T.-Y.; Bell, M.M.; Lee, W.-C.; DesRosiers, A.J. Polygonal eyewall asymmetric during the rapid intensification of hurricane Michael (2018). *Geoph. Res. Let.* **2020**, *47*, e2020GL087919. [CrossRef]
11. Yurchak, B.S. Description of cloud-rain bands in a tropical cyclone by a hyperbolic-logarithmic spiral. *Russ. Meteorol. Hydrol.* **2007**, *32*, 8–18. [CrossRef]
12. Yurchak, B.S. The use of a spiral band model to estimate tropical cyclone intensity. In *Current Topics in Tropical Cyclone Research*; IntechOpen: London, UK, 2019; pp. 1–19. Available online: https://www.intechopen.com/chapters/68590 (accessed on 14 June 2019).
13. Dvorak, V.F. Tropical cyclone intensity analysis and forecasting from satellite imaginary. *Mon. Wea. Rev.* **1975**, *103*, 420–430. [CrossRef]
14. Fernandez, W. Organization and motion of the spiral rainbands in hurricanes: A review. *Cien. Tecn.* **1982**, *6*, 49–98.
15. Willoughby, H.E. The dynamics of the tropical cyclone core. *Austr. Meteorol. Mag.* **1988**, *36*, 183–191.
16. Yurchak, B.S. An estimate of the hurricane's intensity from radar data using hyperbolic-logarithmic approximation. *Int. J. Remote Sens.* **2019**, *40*, 9629–9964. [CrossRef]
17. Yurchak, B.S. Estimating the intensity of hurricanes from historical radar data using the hyperbolic-logarithmic approximation of spiral rainbands. *Adv. Environ. Eng. Res.* **2020**, *1*, 1–13. [CrossRef]
18. Holland, G.J. An analytic model of the wind and pressure profiles in Hurricanes. *Mon. Wea. Rev.* **1980**, *106*, 1212–1218. [CrossRef]
19. Jorgensen, D.P. Mesoscale and convective-scale characteristics of mature hurricanes. Part I: General observations by research aircraft. *J. Atmos. Sci.* **1984**, *41*, 1268–1285. [CrossRef]
20. Franklin, J.L.; Lord, S.J.; Feuer, S.F.; Marks, F.D., Jr. The kinematic structure of Hurricane Gloria (1985) determined from nested analysis of dropwindsonde and Doppler radar data. *Mon. Wea. Rev.* **1993**, *121*, 2433–2451. [CrossRef]
21. Royal Observatory Hong Kong. Tropical Cyclones in 1989—Hong Kong. October 1990. Available online: https://reliefweb.int/sites/reliefweb.int/files/resources/tc1989.pdf (accessed on 10 December 2021).
22. Doviak, R.; Zrnic, D.S. *Doppler Radar and Weather Observations*, 2nd ed.; Academic Press: San Diego, CA, USA, 1993; 562p.
23. Anh, N.X.; Lutsetko, V.I.; Popov, D.O.; Chi, C.P.; Hoai, T.T. Remote sensing of atmosphere and underlying surface using radiation of global navigation satellite systems. *J. Mar. Sci. Technol.* **2017**, *17*, 1–7. Available online: http://www.vjs.ac.vn/index.php/jmst (accessed on 1 February 2022). [CrossRef]
24. Venkataraman, K.S.; Srivastava, H.N.; Chawla, B.K. Radio refractive index variation associated with the passage of two tropical cyclones. *Indian J. Meteorol. Geophys.* **1963**, *14*, 331–333.